Performance Analysis of Bifacial Photovoltaic Modules and Its Practical Implications

Henrik Zsiborács[1,*], Nóra Hegedűsné Baranyai[1], András Vincze[1]

[1]Renewable Energy Research Group, University Center for Circular Economy, University of Pannonia Nagykanizsa, H-8800 Nagykanizsa, Hungary

*Author to whom correspondence should be addressed:
E-mail: zsiboracs.henrik@pen.uni-pannon.hu

(Received March 30, 2026; Revised May 27, 2026; Accepted May 28, 2026)

Abstract: One of the key directions in the development of photovoltaic technologies is increasing the electrical energy yield per unit area, in which bifacial photovoltaic modules are playing an increasingly important role. These modules are characterized by their ability to utilize not only the incident radiation on the front side but also the radiation reaching the rear side, primarily originating from reflection from various surfaces. However, the actual performance gain strongly depends on the installation environment, geometric configuration, and surface reflectivity. The aim of the present study was to provide a quantitative evaluation of bifacial module performance under both real and controlled measurement conditions, with particular emphasis on the separate assessment of front- and rear-side irradiance contributions to electrical power output. The measurements were carried out in Hungary, in the town of Keszthely, under natural conditions with natural grass as ground cover, as well as in controlled configurations using full covering of the module. Based on the field measurements, bifacial operation resulted in an average power increase of 8.7% compared to the monofacial reference. Additional investigations revealed that, under controlled conditions, the electrical response of the rear side reached approximately 73% of the front-side power, which is consistent with the bifaciality factor of the investigated module. The results highlight a significant distinction between the intrinsic, module-level physical potential of bifacial technology and the performance gain that can be practically realized under real installation conditions. From a practical perspective, the applicability of bifacial technology is therefore highly site-specific, and its effective utilization can only be achieved through the combined consideration of installation environment and structural parameters, particularly module mounting height, tilt angle, and the availability of sufficient rear-side clearance.

Keywords: albedo; bifacial photovoltaic modules; component-based measurement; installation geometry; performance analysis; photovoltaic systems; rear-side irradiance

1. Introduction

Over the past decades, the global energy system has undergone significant structural transformation, primarily driven by increasing energy demand, challenges related to the security of production and supply chains, geopolitical uncertainties, and the growing environmental pressures associated with climate change[1–3]. This transformation is further reinforced by the continued growth of global primary energy demand, driven by economic development, urbanization, and population increase[4–6], as well as by international decarbonization efforts, including the IPCC AR6 pathways and SDG7 on affordable and clean energy[7–10]. Consequently, renewable energy technologies have become central to future electricity systems, with solar energy playing a particularly important role because of its broad availability, modularity, and suitability for decentralized generation. Current trends indicate that renewable technologies, particularly wind and solar energy, are expected to further expand their contribution to electricity generation in the long term[11,12].

The rapid proliferation of photovoltaic (PV) systems is closely linked to continuous technological advancements and declining costs, which have made PV increasingly competitive with conventional energy generation technologies in many regions[13,14].

During the development of PV technology, several distinct generations of semiconductor-based solar cells have emerged, including first-generation crystalline silicon (c-Si), second-generation thin-film technologies (e.g., CdTe, CIGS), and third-generation advanced concepts such as perovskite and tandem structures. Among these, crystalline

Cite: H. Zsiborács, N. Hegedűsné Baranyai, A. Vincze, "Performance Analysis of Bifacial Photovoltaic Modules and Its Practical Implications". Evergreen, 13 (02) 801-812 (2026). https://doi.org/10.5109/7432656.

silicon-based systems continue to dominate the market[15–18]. The widespread adoption of PV systems is further supported by their modular design, which enables applications ranging from small-scale residential installations to large utility-scale power plants.

However, one of the fundamental challenges of PV systems arises from their dependence on weather conditions. The temporal and spatial variability of solar irradiance introduces significant uncertainty in energy production, posing challenges for power system integration, including limited predictability of generation, difficulties in maintaining grid stability, and increased demand for system flexibility and energy storage. Consequently, research and development efforts are increasingly focused on improving efficiency, stabilizing energy production, and maximizing the energy yield per unit module area and available land[19–21].

Conventional PV system design is based on monofacial modules, which utilize only the solar radiation incident on their front surface; therefore, their energy production primarily depends on the intensity of direct and diffuse irradiance. In contrast, bifacial PV technology has gained increasing attention in recent years as an advanced development of monofacial systems[22,23]. Bifacial PV modules are capable of utilizing not only the radiation incident on the front side but also the radiation reaching the rear side, which mainly originates from reflected light from surrounding surfaces, thereby increasing the energy yield per unit area[23–25].

Previous experimental, modeling, and review studies have reported that the additional energy yield of bifacial systems typically ranges from a few percent up to approximately 30%, showing a strong dependence on surface reflectivity[23,26–30]. For instance, in low-albedo environments, such as natural soil or vegetation, gains are typically around 5–10%, whereas under highly reflective surface conditions, increases of up to 25–30% can be achieved[23,26–28]. However, the resulting energy yield depends not only on the irradiance incident on both module surfaces but also on the optical and geometric characteristics of the installation environment, including ground reflectivity, module spacing, and tilt angle. Therefore, it is essential to determine the expected performance gain on a site-specific basis, as values reported for specific installation and surface conditions may significantly differ from the actual performance increase under real installation conditions[23,26–31]. Consequently, the performance modeling of bifacial systems is inherently more complex than that of monofacial systems, as, in addition to the conventional direct and diffuse components, the rear-side irradiance must be treated as a separate contribution[32–34].

State-of-the-art modeling approaches decompose the output power into individual irradiance components, accounting for the effects of angle of incidence and temperature corrections, while treating the rear-side power contribution separately[32]. This component represents the energy generation originating from reflected radiation, and its magnitude depends on the bifaciality factor (i.e., the ratio of rear-side to front-side electrical response)[35], as well as on the reflectivity of the surrounding environment. Previous modeling and validation studies have shown that rear-side irradiance cannot be simply described as an extension of diffuse radiation, as its spatial and temporal behavior differs significantly and is strongly influenced by environmental conditions[32–34]. Accordingly, the reliable estimation of bifacial system performance typically requires model parameters to be derived from measurement data, enabling a consistent treatment of the different irradiance components[32].

The development of bifacial technology is closely linked to advancements in modern solar cell architectures, such as Passivated Emitter and Rear Cell (PERC), Tunnel Oxide Passivated Contact (TOPCon), and heterojunction (HJT) structures, which enable efficient dual-side light harvesting and improved conversion efficiencies[36–38].

The economic relevance of bifacial technology is further enhanced by the fact that bifacial modules are increasingly approaching cost parity with monofacial systems, while offering the potential for higher energy yield depending on environmental and installation conditions. This can lead to a reduction in the levelized cost of electricity (LCOE)[23,39,40]. Based on current technological and market trends, the share of bifacial PV systems is steadily increasing, and several industry projections anticipate their continued expansion over the coming decade. Consequently, a detailed understanding of the operation, performance, and optimization potential of bifacial systems is of growing importance for both research and practical applications[22–24].

Based on the above, bifacial PV technology exhibits significant potential for increasing the electrical energy generated per unit area. However, the extent to which this potential can be realized strongly depends on installation conditions, environmental reflectivity, and the geometric configuration of the modules. Since rear-side irradiance can vary substantially with environmental and geometric conditions, the applicability of bifacial technology must be assessed in a site-specific, system-level context[29–31].

At the same time, a reliable interpretation of system-level behavior fundamentally relies on a detailed understanding of the physical processes occurring at the module level, particularly through the separate analysis of front- and rear-side irradiance components[32–34]. Although previous studies have demonstrated the potential performance benefits of bifacial technology under favorable or high-reflectivity conditions[23,26–30], the direct applicability of these findings to real, natural installation environments may be limited.

Based on the technological characteristics and application

Cite: H. Zsiborács, N. Hegedűsné Baranyai, A. Vincze, "Performance Analysis of Bifacial Photovoltaic Modules and Its Practical Implications". Evergreen, 13 (02) 801-812 (2026). https://doi.org/10.5109/7432656.

conditions outlined above, the present study focuses on the quantitative analysis of bifacial module performance. Particular emphasis is placed on the separate evaluation of power components originating from front- and rear-side irradiance. A key source of uncertainty in bifacial performance estimation is the rear-side contribution under realistic operating conditions, which cannot be reliably inferred from nominal bifaciality factors or generalized literature values alone. Therefore, component-separated measurements are essential not only for directly quantifying the rear-side power component, but also for providing experimental validation data for bifacial performance assessment and modeling. Accordingly, one of the primary objectives of this study is to assess the extent to which rear-side contributions measured under real, natural albedo conditions deviate from the ranges reported in previous studies[23,26–30].

The central hypothesis is that the intrinsic rear-side response of a bifacial module, determined under controlled component-separated conditions, can substantially differ from the performance gain realized under natural low-albedo operating conditions. To test this hypothesis, field measurements under natural grass-covered conditions were combined with controlled covering configurations that isolate front- and rear-side power components. This approach enables the direct comparison of front- and rear-side power components of a PV module and clarifies the difference between module-level physical potential and practically achievable performance gain, thereby supporting a more realistic engineering assessment of bifacial PV installations.

2. Materials and methods

The following two subsections present the experimental methodology applied for the investigation of bifacial PV module performance, including the measurement conditions, the experimental setup, and the instrumentation used for recording electrical and environmental parameters. The applied measurement configurations, namely real environmental conditions and controlled fully covered arrangements, enabled the separate and quantitative evaluation of front- and rear-side power components.

2.1. Experimental setup and measurement conditions

This section describes the experimental conditions and measurement configurations applied in the study. For clarity, the setup is presented in three parts: site and measurement timing, module selection and installation geometry, and experimental configurations.

2.1.1. Experimental site and measurement timing

The measurements were carried out in Hungary, in the town of Keszthely (46.7675° N, 17.2661° E), which is characterized by a temperate continental climate and can be considered representative for Central European PV applications.

The measurements were conducted on three separate days in May and June 2025: May 21 (12:15–14:00), May 22 (11:30–12:00), and June 13 (12:15–13:15). Continuous data acquisition was applied in all cases. The primary objective of selecting these time periods was not to determine total daily or seasonal energy yield, but to investigate module-level behavior under high irradiance and ideal weather conditions (clear sky, cloud-free). These conditions ensured that the measured results represent the near-maximum operating states of the bifacial modules while minimizing uncertainties arising from variable meteorological factors, thereby improving the comparability of different measurement configurations (e.g., grass-covered surface and controlled full cover).

During each measurement window, multiple repeated observations and configuration changes were performed, while environmental and electrical parameters were continuously monitored. Conducting the measurements on multiple independent days allowed the verification of reproducibility under similar high-irradiance conditions. In addition, long continuous measurement periods and high sampling frequency provided a substantial number of repeated observations for the evaluation of each configuration.

During data evaluation, instead of using averages over the entire measurement period, only those time intervals were selected in which irradiance and environmental conditions could be considered nearly constant (quasi-stationary conditions). Within these intervals, the system exhibited stable operation, and electrical power was determined based on short observation periods (typically 10–20 s), representing the quasi-stationary operating state characteristic of each configuration. This approach enabled the analysis of bifacial module performance under operating conditions corresponding to high irradiance levels. Within the selected quasi-stationary intervals, electrical power remained stable at the applied measurement resolution, while front- and rear-side irradiance varied only slightly, typically within approximately 1–2 W/m². Since the selected intervals represented stable operating states, standard deviations were calculated from the independent measurement days to characterize day-to-day variability rather than fluctuations within the short quasi-stationary intervals.

2.1.2. Module selection and installation geometry

The study was based on ground-mounted bifacial PV technology, and the investigation focused on module-level measurements, as the primary objective was to examine the physical and radiative phenomena directly associated with bifacial operation at the module and its immediate surroundings. Accordingly, the analysis did not aim to evaluate system- or string-level performance, but rather to

Cite: H. Zsiborács, N. Hegedűsné Baranyai, A. Vincze, "Performance Analysis of Bifacial Photovoltaic Modules and Its Practical Implications". Evergreen, 13 (02) 801-812 (2026). https://doi.org/10.5109/7432656.

provide a detailed assessment of module-level behavior, with particular emphasis on energy generation characteristics arising from bifacial irradiance.

The investigated system consisted of four bifacial modules with identical technical specifications, whose performance was evaluated under operating conditions. Preliminary comparative measurements revealed only negligible differences among the modules; therefore, their behavior was considered representative. This step also served to verify measurement stability and reproducibility. Consequently, the detailed measurement and analysis focused on a single selected module, which proved suitable for characterizing the overall system behavior. The selection of this module was not based on predefined criteria, as no significant performance differences were observed among the modules, thus any unit could be considered representative.

The modules were installed with southern orientation and a tilt angle of 35°, which is considered close to optimal for maximizing annual energy yield under Hungarian climatic conditions[41].

For measurements conducted on a grass-covered surface, two identical mobile mounting structures were constructed (Figure 1), of which one was used in the present study. The mounting system allowed the adjustment of the tilt angle; however, a fixed tilt of 35° was applied in all measurements. In this configuration, the lower edge of the module was positioned 1 m above ground level, ensuring a setup representative of real installation conditions while promoting a more uniform distribution of rear-side irradiance and more effective utilization of ground-reflected radiation, which is of key importance for bifacial operation[35].

For rear-side measurements, the module was removed from the mounting structure and placed directly on the ground. This approach was necessary both to avoid shading effects and to ensure safe handling, as stable fixation of the inverted configuration on the mounting structure could not be guaranteed and would have posed a risk of damage to the glass surface of the module.

Fig. 1: Mobile mounting structure used for the investigation of the bifacial PV module

2.1.3. Experimental configurations

The surface behind the module differed between measurement configurations and represented different environmental conditions: on the one hand, a natural, vegetation-covered (grass) surface, and on the other hand, a controlled configuration in which the front- and rear-side irradiance of the module was modified through complete covering. The controlled (fully covered) measurements were carried out in May, while the measurements under natural (grass-covered) conditions were performed on all three measurement days, as the controlled experiments showed consistent behavior.

In the controlled covering configurations, one side of the module was fully covered at a time, allowing the electrical response associated with the exposed side to be recorded separately. In the case of complete covering, the effect of albedo was not considered, since the module was operated under a monofacial reference condition. The natural grass-covered measurements and the controlled covering configurations were therefore treated as separate measurement cases during data evaluation.

For the grass-covered surface, reflected irradiance was measured using a pyranometer (see Section 2.2), oriented according to the tilt angle of the module and directed both towards the sky and the ground. Therefore, the measurements represent plane-of-module irradiance components rather than global horizontal irradiance. It should be noted that a dedicated albedometer or horizontal up-/down-facing pyranometer configuration was not used in this study; therefore, the measured reflected/incident ratio should not be interpreted as strict surface albedo. Instead, it represents an effective rear/front irradiance ratio in the module plane, which is directly relevant to the bifacial operating configuration investigated here. According to literature data, the albedo of grass typically ranges between 0.15 and 0.25, and may reach values up to 0.26 in the case of fresh grass[42].

2.1.4. Methodological positioning relative to previous studies

To place the present case study in the context of earlier bifacial PV research, Table 1 summarizes selected studies according to their methodological approach, installation or surface focus, and relevance to the present experimental design. This comparison highlights that the present study combines natural grass-covered field measurements with controlled component-separated measurements, thereby enabling a direct distinction between practical performance gain and module-level rear-side response.

Table 1: Methodological comparison of the present case study with selected previous bifacial PV studies

Study	Methodological approach	Installation / surface focus	Main relevance to bifacial PV assessment	Contribution to bifacial PV assessment
Yakubu et al. 2024 [23]	Systematic literature review	Broad range of bifacial PV applications	Summarizes major factors affecting bifacial PV performance and applications	Provides general context for the need for site-specific bifacial assessment
Gu et al. 2020 [26]	Review and technology outlook	Different bifacial PV configurations and operating conditions	Highlights the dependence of bifacial gain on environmental and system parameters	Supports the interpretation that generalized bifacial gains cannot be directly transferred to all sites
Sun et al. 2018 [27]	Modeling and global performance analysis	Different albedo and mounting conditions	Shows the importance of albedo and installation configuration for bifacial gain	Supports the site-specific interpretation of bifacial performance
Dincer and Ozer, 2025 [29]	Parametric analysis	Albedo, tilt, height, and mounting configuration	Evaluates the sensitivity of rear-side contribution to installation geometry	Supports the focus on module height, tilt angle, and surface reflectivity
Alam et al. 2023 [30]	Performance comparison under different ground albedo conditions	Different ground-reflectivity cases	Demonstrates the influence of ground albedo on bifacial performance gain	Confirms the relevance of reflected-irradiance measurements under different ground-reflectivity conditions
Brecl et al. 2025 [32]	Bifacial PV performance modeling	Direct and diffuse irradiance components	Treats bifacial performance through component-based irradiance and power modeling	Supports the need for measurement data that can help validate component-based performance assessment
Ernst et al. 2024 [34]	Bifacial irradiance modeling and validation	View-factor and ray-tracing approaches	Compares and validates approaches for modeling bifacial irradiance	Supports the relevance of separating front- and rear-side irradiance contributions
Present study	Field measurements and controlled covering measurements	Natural grass-covered surface in Keszthely, Hungary; controlled front-/rear-side covering configurations	Separates practical field gain from module-level rear-side response	Provides direct component-separated experimental evidence for a Central European natural grass-covered case study

2.2. Measurement system and instrumentation

The measurement system was designed to enable the simultaneous recording of bifacial PV module operation and the associated environmental parameters with high temporal resolution.

The system consisted of a CR1000 data logger[43] and a DS-2 ultrasonic anemometer (Figure 2)[44] connected to it. The CR1000 ensured continuous and reliable acquisition of sensor data under field conditions, while the DS-2 ultrasonic anemometer provided supplementary data related to air temperature[45]. The data acquisition was performed with a one-minute sampling interval.

The module temperature was determined using a Testo 872s thermal imaging camera[46] , which enabled the non-contact measurement of the module surface temperature, as well as the assessment of local temperature distributions and potential inhomogeneities. The temperature data were primarily used for qualitative interpretation.

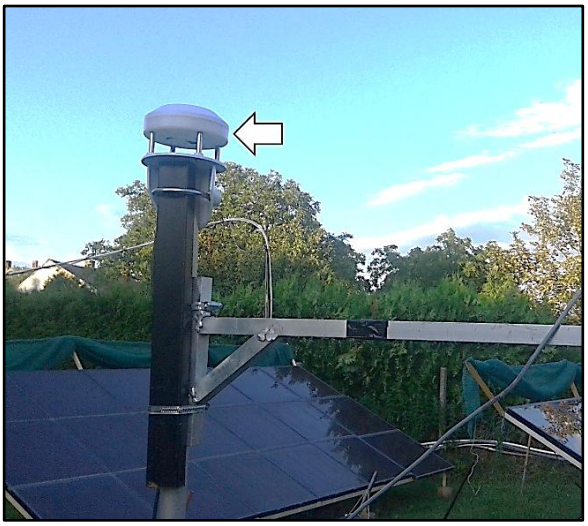

Fig. 2: Measurement setup of the DS-2 ultrasonic anemometer

Incoming and reflected irradiance were measured using two Hukseflux LP02 pyranometers[47]. The LP02 sensors were used to determine irradiance components in the plane of the module. The sensors were installed according to the tilt angle of the module, with the same orientation as the module plane, thereby measuring plane-of-module irradiance components from both the sky and the ground, under identical geometric conditions. The use of two sensors enabled the separate and accurate determination of incident and reflected radiation components, while the measurement uncertainty was typically ±1–3% according to the sensor specifications.

The pyranometer signals were recorded using a four-channel HOBO analog data logger[48], which enabled 1 s temporal resolution for tracking irradiance conditions. The voltage signals measured by the pyranometers were converted into irradiance values using the sensitivity (calibration) factors provided by the manufacturer. No additional statistical filtering or modeling was applied during data processing.

The electrical power output of the PV module was determined using a Victron Energy SmartSolar MPPT 75/15 charge controller[49]. The device is equipped with built-in Bluetooth communication, enabling real-time monitoring of operating parameters (voltage, current, and power) with 1 s temporal resolution via the application provided by the manufacturer. During the measurements, the system was connected to two Banner Energy Bull batteries (12 V nominal voltage, 60 Ah capacity) connected in series[50], forming a 24 V system. The charge controller was selected to ensure that its maximum power handling capacity (440 W at 24 V) provided sufficient margin relative to the nominal power of the investigated 370 W bifacial module, thereby covering the full operational range. The applied Maximum Power Point Tracking (MPPT) control enables continuous operation of the module at its maximum power point under varying irradiance and temperature conditions. The MPPT control allowed the module to operate near its maximum power point during the selected quasi-stationary intervals.

For data synchronization, the HOBO irradiance data and MPPT electrical data recorded with 1 s temporal resolution were used to identify quasi-stationary 10–20 s evaluation intervals. The one-minute CR1000/anemometer air-temperature data were synchronized to these intervals using timestamps, with the nearest time-matched temperature value assigned to each interval. Intervals were retained only when irradiance and electrical power remained stable.

The investigated PV module was a JA Solar JAM72D00-370/BP bifacial, glass–glass monocrystalline PERC module[51], with a nominal power of 370 W under standard test conditions. The main electrical parameters of the module include an open-circuit voltage (Voc) of 48.44 V and a short-circuit current (Isc) of 9.80 A, which are essential for interpreting system performance. The bifaciality factor of the module is 70% ± 5%, indicating that the rear-side energy conversion can reach a substantial fraction of the front-side performance under appropriate irradiance conditions. The temperature coefficient of power is −0.380%/°C, indicating a decrease in module performance with increasing temperature, thus highlighting the importance of thermal conditions in real operating performance.

To consolidate the instrumentation and data acquisition procedure, the main sensors, acquisition systems, sampling intervals, and relevant specifications are summarized in Table 2.

Table 2: Summary of measurement devices and data acquisition parameters

Parameter	Device / sensor	Acquisition system	Sampling interval / resolution	Uncertainty / key specification	Role in the study
Air temperature	DS-2 ultrasonic anemometer	CR1000 data logger	1 min	Manufacturer specification	Supplementary environmental parameter
Module surface temperature	Testo 872s thermal imaging camera	Thermal imaging	Measurement-campaign dependent	Manufacturer specification	Qualitative assessment of module temperature distribution
Incident and reflected irradiance	Two Hukseflux LP02 pyranometers	HOBO four-channel analog data logger	1 s	Typically ±1–3%	Determination of plane-of-module irradiance components from sky and ground directions
Electrical parameters	Victron Energy SmartSolar MPPT 75/15	Manufacturer application via Bluetooth	1 s	Maximum efficiency up to 98%	Determination of module voltage, current, and electrical power
PV module	JA Solar JAM72D00-370/BP bifacial glass–glass PERC module	—	—	370 W nominal power; bifaciality factor 70% ± 5%; power temperature coefficient −0.380%/°C	Investigated bifacial PV module

Cite: H. Zsiborács, N. Hegedűsné Baranyai, A. Vincze, "Performance Analysis of Bifacial Photovoltaic Modules and Its Practical Implications". Evergreen, 13 (02) 801-812 (2026). https://doi.org/10.5109/7432656.

3. Results and discussions

The experimental results are presented in two parts. First, the effect of the rear-side irradiance under natural grass-covered conditions is evaluated by comparing the bifacial operation with the monofacial reference case, indicating the practical performance gain achievable in a low-albedo environment. Second, the front- and rear-side power components are analyzed separately under controlled covering conditions, providing a direct basis for interpreting the module-level rear-side response.

3.1. The effect of rear-side irradiance on module performance

Figure 3 shows the measurement setup used to evaluate the bifacial PV module under real environmental conditions.

The measurement results clearly demonstrate that the presence of rear-side irradiance increased the electrical power output of the module in all investigated cases.

Across the three independent measurement days, the electrical power increased from 308 W to 336 W, from 306 W to 333 W, and from 297 W to 321 W when comparing the monofacial reference condition (rear side covered) to bifacial operation (rear side exposed). These correspond to performance increases of 9.1%, 8.8%, and 8.1%, respectively, with an average increase of 8.7% and a standard deviation of 0.5 percentage points among the three independent measurement days, corresponding to a coefficient of variation of approximately 5.7%. The consistency of the results is particularly noteworthy, as only minimal variation was observed between different measurement periods and environmental conditions.

During the measurements on the grass-covered surface, the rear-side irradiance ranged between 77 and 102 W/m², while the front-side irradiance was approximately 938–977 W/m² (Table 3). The resulting reflected/incident ratio varied between 0.082 and 0.105, with an average value of ~0.097. This value can be interpreted as an effective rear/front irradiance ratio for the given measurement configuration. Although it is not identical to the strict definition of surface albedo, the ratio characterizes the irradiance actually available to the rear side of the inclined bifacial module under the investigated operating configuration.

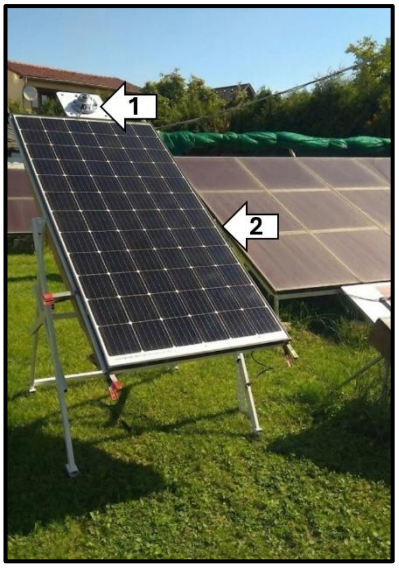

Fig. 3: The measurement setup of the bifacial PV module under real environmental conditions (1: Hukseflux LP02 pyranometer; 2: JA Solar JAM72D00-370/BP PV module)

The results indicate that, under real environmental and geometric conditions, the observed performance gain may exceed the typically reported ~5–6% values associated with low-albedo (~0.15) grass-covered surfaces [28]. The measured average increase of ~8.7% is more consistent with previously reported values for higher albedo conditions (~0.25), where gains approaching ~10% are expected. This suggests that the albedo of grass can vary significantly depending on environmental conditions, and that more favorable surface characteristics can substantially enhance rear-side electrical output.

At the same time, the results highlight that the actual performance gain in practical applications is not determined solely by nominal albedo values, but also by site-specific geometric factors, including module height, tilt angle, and the combined effects of diffuse and reflected irradiance components. Overall, the measured results show

Table 3: Performance comparison between monofacial and bifacial operation

Date	21.05.2025	22.05.2025	13.06.2025
Measurement interval	12:15-14:00	11:30-12:00	12:15-13:15
Average module temperature (°C)	52	53	57
Front-side irradiance (W/m²)	977	975	938
Rear-side irradiance (W/m²)	102	102	77
Monofacial power (W)	308	306	297
Bifacial power (W)	336	333	321
Rear-side power contribution (W)	28	27	24
Performance increase relative to the monofacial reference (%)	9.1	8.8	8.1
Average performance increase relative to the monofacial reference (%)		8.7	
Standard deviation of performance increase among the three measurement days (percentage points)		0.5	

Cite: H. Zsiborács, N. Hegedűsné Baranyai, A. Vincze, "Performance Analysis of Bifacial Photovoltaic Modules and Its Practical Implications". Evergreen, 13 (02) 801-812 (2026). https://doi.org/10.5109/7432656.

qualitative agreement and quantitative consistency with previously reported trends regarding the relationship between albedo, installation geometry, rear-side irradiance, and bifacial performance[23,26,27,29,30].

3.2. The component-based analysis of the bifacial module performance

A component-based analysis of electrical power was carried out using controlled fully covered configurations to directly compare the front- and rear-side power components. This approach allowed the rear-side electrical response to be quantified separately from the total bifacial performance gain observed under real environmental conditions.

Two different measurement configurations were applied (Figure 4). In the first case, the rear side of the module was covered, and thus the measured electrical power originated exclusively from front-side irradiance. This configuration served as a reference condition, representing operation close to that of a conventional monofacial module.

In the second configuration, the module was inverted while maintaining the same geometric arrangement, and the front side was covered. This setup enabled the direct determination of the electrical power potential associated with rear-side irradiance. Under these conditions, the measured electrical output represents the rear-side response under direct irradiation, allowing this component of bifacial operation to be quantified independently under controlled conditions.

The covering blocked incident radiation on the covered side; therefore, these measurements were used only for controlled side-by-side comparison and not as a representation of real operating conditions.

The results clearly indicate the dominant role of front-side operation. The measured electrical power values ranged between 303 and 304 W under nearly identical irradiance conditions of approximately 972–974 W/m². This demonstrates that the module response under front-side irradiance was stable and highly reproducible, accurately representing a quasi-stationary operating state under high irradiance conditions.

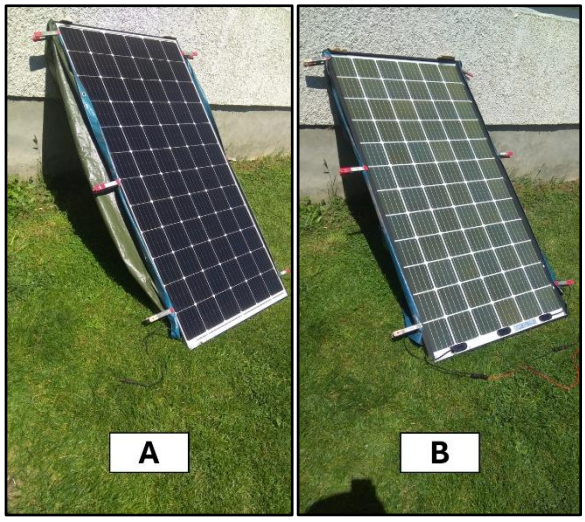

Fig. 4: The controlled fully covered configurations for the component-based evaluation of the front-side and rear-side power in the bifacial module (A: rear side covered; B: front side covered)

In contrast, the electrical power measured for the rear side was significantly lower, with values between 221 and 222 W (Table 4). These results reflect the controlled operation with direct rear-side irradiance and do not represent real operating conditions. However, the lower power output does not indicate negligible rear-side contribution, but rather a physically justified difference arising from the bifacial module design, as the rear-side light conversion efficiency is typically lower than that of the front side. Importantly, the results demonstrate that under favorable irradiance conditions, the rear side alone is capable of delivering a substantial level of electrical power.

Based on the measurements, the rear-side power reached approximately 73% of the front-side output under controlled conditions, which is in good agreement with the bifaciality factor of the investigated module (~70%). The ratio derived from the measured values (221–222 W vs. 303–304 W, ~0.73) indicates that the rear-side electrical response closely follows the manufacturer's specifications. These findings confirm that the rear-side performance of the module is physically consistent with its specified characteristics, and that the measured values provide a realistic representation of the electrical contribution associated with bifacial operation.

The results of the component-based analysis not only support the qualitative interpretation of bifacial operation but also enable a clear distinction between the physical potential of the technology and the performance gain achievable under real environmental conditions. While the measurements conducted under natural grass-covered conditions (Section 3.1) showed an average performance increase of approximately ~8–9% attributable to rear-side contribution, the controlled experimental configuration revealed that the rear side alone can produce up to ~73%

Table 4: The comparison of the front-side and rear-side power under monofacial and bifacial operation

Date	21.05.2025	22.05.2025
Measurement interval	12:15–14:00	11:30–12:00
Average module temperature (°C)	54	53
Front-side irradiance (W/m²)	972	974
Front-side power (W) (rear side covered)	303	304
Rear-side power (W) (front side covered)	222	221
Rear/front power ratio (%)	73.3	72.7

Cite: H. Zsiborács, N. Hegedűsné Baranyai, A. Vincze, "Performance Analysis of Bifacial Photovoltaic Modules and Its Practical Implications". Evergreen, 13 (02) 801-812 (2026). https://doi.org/10.5109/7432656.

of the front-side power under direct illumination.

However, it is important to emphasize that this ratio cannot be directly interpreted as a realistic performance gain under actual operating conditions. The observed ~73% ratio reflects the intrinsic electrical response capability of the rear side under given irradiance conditions and is closely related to the bifaciality factor of the module, but it does not represent a system-level performance increase. In practical applications, the rear-side contribution to the total power output is typically significantly lower, and even under favorable installation conditions, the achievable gain rarely exceeds ~30%.

In addition to albedo and installation geometry, angle-of-incidence (AOI) and spectral effects may also influence rear-side performance. The measurements in the present study were conducted during midday periods under high-irradiance conditions, corresponding to relatively favorable AOI conditions for the investigated fixed-tilt configuration. Under low sun-angle conditions, AOI-related optical losses may become more pronounced, and the angular distribution of rear-side irradiance may differ from that of front-side irradiance because the rear side receives a combination of ground-reflected and diffuse radiation. This is particularly relevant for bifacial PV modules, where incidence-angle effects are influenced by both front-side beam irradiance and rear-side reflection[52]. Furthermore, vegetation-covered surfaces may modify the spectral composition of reflected irradiance, while crystalline silicon PV modules and broadband pyranometers do not necessarily have identical spectral responses. Therefore, spectral mismatch may affect the relationship between measured rear-side irradiance and the effective irradiance converted by the module. Since spectral irradiance was not measured in the present study, the reflected/incident ratio should be interpreted as a broadband plane-of-module irradiance ratio rather than a spectrally resolved rear-side contribution[53].

These findings show that the evaluation of bifacial PV systems cannot rely solely on module specifications or bifaciality factors, but must also account for site-specific environmental and geometric conditions. The present results confirm that in low-albedo natural environments, the performance gain remains moderate, whereas higher-reflectivity or optimized configurations may allow the advantages of bifacial operation to be utilized more effectively.

4. Conclusions and future scope

The results demonstrated that under natural, low-albedo grass-covered conditions, bifacial operation provides a stable and reproducible performance gain, averaging approximately 8.7% relative to the monofacial reference case. In addition, the component-based analysis revealed that under controlled conditions the rear side alone can reach approximately 73% of the front-side power, corresponding to the bifaciality factor of the investigated module. However, this value does not represent a realistic performance gain under actual operating conditions but rather illustrates the intrinsic physical potential of the module and, more generally, that of the bifacial design.

The combined application of real-environment and controlled measurement approaches clearly highlights the substantial difference between the theoretical technical potential and the performance gain that can be effectively realized under site-specific installation conditions. These findings emphasize that bifacial gains are strongly dependent on site-specific and geometric conditions, particularly rear-side clearance, mounting height, tilt angle, and surface reflectivity.

From a practical perspective, the present study also points out that the application of bifacial modules can only be considered justified if the installation configuration allows for a meaningful contribution from rear-side irradiance.

In configurations where modules are mounted close to a surface, such as on pitched roofs or inclined roof planes with minimal rear-side clearance, the utilization of rear-side irradiance is significantly limited. In such cases, the advantages of bifacial design may be negligible. In contrast, ground-mounted systems with sufficient height, favorable surface reflectivity, and optimized geometric configuration, as well as flat-roof installations with adequate rear-side clearance, offer conditions under which the benefits of bifacial technology can be effectively exploited. In these configurations, the artificial enhancement of surface reflectivity may further increase performance; however, its practical applicability must also consider maintenance requirements, as maintaining high albedo may require regular cleaning or surface treatment.

From an engineering perspective, it is also important to consider that bifacial modules, particularly those with glass–glass construction, typically have higher weight compared to conventional monofacial modules. This has implications for mounting structure design, roof load capacity, fixation methods, and overall installation planning. Therefore, the deployment of bifacial technology requires careful technical and economic assessment in each specific case.

Based on the present results, it can be concluded that the applicability of bifacial modules cannot be generalized, but it is strongly dependent on whether the specific installation environment enables effective rear-side energy utilization. Future research should focus on the geometric optimization of ground-mounted bifacial systems, particularly investigating how the spacing between adjacent modules influences rear-side irradiance and overall energy yield. In parallel, longer-term measurements under different climatic, surface-reflectivity, vegetation, moisture, and mounting conditions would allow the site-specific findings of the present case study to

Cite: H. Zsiborács, N. Hegedűsné Baranyai, A. Vincze, "Performance Analysis of Bifacial Photovoltaic Modules and Its Practical Implications". Evergreen, 13 (02) 801-812 (2026). https://doi.org/10.5109/7432656.

be evaluated across a broader range of operating conditions. Future studies should also compare module technologies with different bifaciality factors, as this would help determine how strongly the observed distinction between intrinsic rear-side response and practical field gain depends on the specific module design. Another important research direction is the analysis of shading sensitivity in bifacial systems, with particular emphasis on partial shading effects and hotspot formation mechanisms. Such investigations can contribute to more robust system design, not only from an energy yield perspective, but also in terms of operational reliability and long-term performance.

Acknowledgements

We acknowledge the financial support of 2021-1.2.6-TÉT-IPARI-MA-2022-00025 financed from the National Research, Development and Innovation Office (NRDI) Fund.
The authors would like to thank Henrik Zsiborács Sr. and István Zsiborács for their valuable support.

Contributions

H. Zsiborács: Concept, design, and performance of the experiments, conceptualization, data curation, methodology, supervision, validation, writing of original draft, writing, review & editing. N. Hegedűsné Baranyai: conceptualization, data curation, methodology, supervision, validation, writing original draft, writing, review & editing. A. Vincze: methodology, supervision, validation, writing original draft, writing, review & editing.

Declaration of competing interests

The authors declare no conflict of interest.

References

1) D. Chatzinikolaou, and C.M. Vlados, “New globalization and energy transition: insights from recent global developments,” Societies 2024, Vol. 14, 14 (9) (2024). doi:10.3390/soc14090166.
2) Y. Yang, S. Xia, and X. Qian, “Geopolitics of the energy transition,” Journal of Geographical Sciences 2023 33:4, 33 (4) 683–704 (2023). doi:10.1007/s11442-023-2101-2.
3) Z. Zhu, A.I. Hunjra, S.S. Alharbi, and S. Zhao, “Global energy transition under geopolitical risks: an empirical investigation,” Energy Econ., 145 108495 (2025). doi:10.1016/j.eneco.2025.108495.
4) J. Liu, M. Yin, K. Wang, J. Zou, and Y. Kong, “Long-term impacts of urbanization through population migration on china’s energy demand and co2 emissions,” Mitigation and Adaptation Strategies for Global Change 2020 25:6, 25 (6) 1053–1071 (2020). doi:10.1007/s11027-020-09919-0.
5) R. Avtar, S. Tripathi, A.K. Aggarwal, and P. Kumar, “Population–urbanization–energy nexus: a review,” Resources 2019, Vol. 8, 8 (3) (2019). doi:10.3390/resources8030136.
6) Q. Wang, M. Su, R. Li, and P. Ponce, “The effects of energy prices, urbanization and economic growth on energy consumption per capita in 186 countries,” J. Clean. Prod., 225 1017–1032 (2019). doi:10.1016/j.jclepro.2019.04.008.
7) I.B. Boa Morte, O. de Q.F. Araújo, C.R.V. Morgado, and J.L. de Medeiros, “Electrification and decarbonization: a critical review of interconnected sectors, policies, and sustainable development goals,” Energy Storage and Saving, 2 (4) 615–630 (2023). doi:10.1016/j.enss.2023.08.004.
8) S. Karlilar Pata, and M. Balcilar, “Decarbonizing energy: evaluating fossil fuel displacement by renewables in oecd countries,” Environmental Science and Pollution Research 2024 31:21, 31 (21) 31304–31313 (2024). doi:10.1007/s11356-024-33324-8.
9) U.K. Pata, “Decarbonization efforts under the energy and climate policy uncertainties: a comparison between the usa and china,” Clean Technologies and Environmental Policy 2024 27:6, 27 (6) 2395–2414 (2024). doi:10.1007/s10098-024-02992-y.
10) K. Calvin, D. Dasgupta, G. Krinner, A. Mukherji, P.W. Thorne, C. Trisos, J. Romero, M. Ha, et al., “IPCC, 2023: climate change 2023: synthesis report. contribution of working groups i, ii and iii to the sixth assessment report of the intergovernmental panel on climate change [core writing team, h. lee and j. romero (eds.)]. ipcc, geneva, switzerland.,” (2023). doi:10.59327/IPCC/AR6-9789291691647.
11) Q. Hassan, S. Algburi, A.Z. Sameen, H.M. Salman, and M. Jaszczur, “A review of hybrid renewable energy systems: solar and wind-powered solutions: challenges, opportunities, and policy implications,” Results in Engineering, 20 101621 (2023). doi:10.1016/J.RINENG.2023.101621.
12) M. Khaleel, Z. Yusupov, and S. Rekik, “Exploring trends and predictions in renewable energy generation,” Energy 360, 4 100030 (2025). doi:10.1016/J.ENERG.2025.100030.
13) N.H. Johari, W.S. Alaloul, and M.A. Musarat, “Recent advancements of life cycle cost analysis of photovoltaic systems: a systematic review,” International Journal of Life Cycle Assessment, 30 (12) 3459–3499 (2025). doi:10.1007/S11367-025-02474-3/METRICS.
14) J. Liu, and X. Shen, “Global pv supply chains: costs and energy savings, ghg emissions reductions,” Energy Policy, 205 114716 (2025). doi:10.1016/J.ENPOL.2025.114716.

15) E. Raza, and Z. Ahmad, “Review on two-terminal and four-terminal crystalline-silicon/perovskite tandem solar cells; progress, challenges, and future perspectives,” Energy Reports, 8 5820–5851 (2022). doi:10.1016/J.EGYR.2022.04.028.
16) G. Yang, C. Deng, C. Li, T. Zhu, D. Liu, Y. Bai, Q. Chen, J. Huang, and G. Li, “Towards efficient, scalable and stable perovskite/silicon tandem solar cells,” Nature Photonics 2025 19:9, 19 (9) 913–924 (2025). doi:10.1038/s41566-025-01732-y.
17) A.A. Ugochukwu, F. Ahmad, M. Khalid, M.A. Ali, I. Mamoon, S.C. Udensi, U. Ogbonna, A. Iqbal, R. Ali, M. Usman, J. Khan, I. Khurshid, U. Zahoor, A.H. shah, A.U. Rahman, and F. Rehman, “Recent enhancement in photovoltaic cell efficiency performance, stability, and cost reduction: a review,” Solar Energy, 300 113853 (2025). doi:10.1016/J.SOLENER.2025.113853.
18) Fraunhofer Institute for Solar Energy Systems ISE., “Photovoltaics Report,” Freiburg, Germany, 2025.
19) E. Ejuh Che, K. Roland Abeng, C.D. Iweh, G.J. Tsekouras, and A. Fopah-Lele, “The impact of integrating variable renewable energy sources into grid-connected power systems: challenges, mitigation strategies, and prospects,” Energies 2025, Vol. 18, Page 689, 18 (3) 689 (2025). doi:10.3390/EN18030689.
20) Y. Ma, Y. Huang, and Y. Yuan, “The short-term intermittency evaluation of distributed photovoltaic power,” Heliyon, 10 (13) e33547 (2024). doi:10.1016/J.HELIYON.2024.E33547.
21) G. Rajendran, R. Raute, and C. Caruana, “A comprehensive review of solar pv integration with smart-grids: challenges, standards, and grid codes,” Energies 2025, Vol. 18, Page 2221, 18 (9) 2221 (2025). doi:10.3390/EN18092221.
22) D. Keiner, L. Walter, D. Bogdanov, I.M. Peters, and C. Breyer, “Assessing the impact of bifacial solar photovoltaics on future power systems based on capacity-density-optimised power plant yield modelling,” Solar Energy, 295 113543 (2025). doi:10.1016/J.SOLENER.2025.113543.
23) R.O. Yakubu, L.D. Mensah, D.A. Quansah, and M.S. Adaramola, “A systematic literature review of the bifacial photovoltaic module and its applications,” The Journal of Engineering, 2024 (8) (2024). doi:10.1049/TJE2.12421.
24) A. Garrod, and A. Ghosh, “A review of bifacial solar photovoltaic applications,” Frontiers in Energy, 17 (6) 704–726 (2023). doi:10.1007/s11708-023-0903-7.
25) R. Guerrero-Lemus, R. Vega, T. Kim, A. Kimm, and L.E. Shephard, “Bifacial solar photovoltaics – a technology review,” Renewable and Sustainable Energy Reviews, 60 1533–1549 (2016). doi:10.1016/j.rser.2016.03.041.
26) W. Gu, T. Ma, S. Ahmed, Y. Zhang, and J. Peng, “A comprehensive review and outlook of bifacial photovoltaic (bpv) technology,” Energy Convers. Manag., 223 113283 (2020). doi:10.1016/j.enconman.2020.113283.
27) X. Sun, M.R. Khan, C. Deline, and M.A. Alam, “Optimization and performance of bifacial solar modules: a global perspective,” Appl. Energy, 212 1601–1610 (2018). doi:10.1016/j.apenergy.2017.12.041.
28) LG Electronics Inc., “2018 PRODUCT CATALOG,” Seoul, Korea, 2018.
29) F. Dincer, and E. Ozer, “Optimization of rear-side energy contribution in bifacial pv panels: a parametric analysis on albedo, tilt, height, and mounting configuration,” Energies 2025, Vol. 18, Page 4443, 18 (16) 4443 (2025). doi:10.3390/EN18164443.
30) M. Alam, M.S. Gul, and T. Muneer, “Performance analysis and comparison between bifacial and monofacial solar photovoltaic at various ground albedo conditions,” Renewable Energy Focus, 44 295–316 (2023). doi:10.1016/J.REF.2023.01.005.
31) X. Su, C. Luo, X. Chen, J. Ji, Y. Yu, Y. Wu, and W. Zou, “Numerical modeling of all-day albedo variation for bifacial pv systems on rooftops and annual yield prediction in beijing,” Build. Simul., 17 (6) 955–964 (2024). doi:10.1007/S12273-024-1120-Y/METRICS.
32) K. Brecl, M. Bokalič, A. Faes, and M. Topič, “An accurate bifacial pv module energy performance model using a direct-diffuse power rating model,” Appl. Energy, 382 (3) 125310 (2025). doi:10.1016/j.apenergy.2025.125310.
33) M. Alam, M.S. Gul, and T. Muneer, “Ground view factor computation model for bifacial photovoltaic collector field: uniform and non-uniform surfaces,” Energy Reports, 7 9133–9149 (2021). doi:10.1016/j.egyr.2021.11.206.
34) M. Ernst, C.A. Asselineau, P. Tillmann, K. Jäger, and C. Becker, “Modelling bifacial irradiance – step-by-step comparison and validation of view factor and ray tracing models,” Appl. Energy, 369 123574 (2024). doi:10.1016/J.APENERGY.2024.123574.
35) LG Electronics Inc., “Bifacial Design Guide,” 2017.
36) K.V. Joseph, N.M. Rosana, J.A. Kumar, and A. V. Samrot, “Commercial bifacial silicon solar cells - characteristics, module topology and passivation techniques for high electrical output: an overview,” Results in Engineering, 26 104971 (2025). doi:10.1016/J.RINENG.2025.104971.
37) J.W. Sohn, M. Woo, S. Lee, S.B. Hong, H. Jang, Y.S. Kim, J. Song, Y. Choe, H.S. Lee, D. Kim, S. Hwang, and Y. Kang, “Performance comparison between

bifacial perc and topcon on a south-facing vertical structure," Energy Sci. Eng., 13 (11) 5566–5573 (2025). doi:10.1002/ESE3.70264.

38) H. Jang, S. Lee, H. Lee, D. Choi, H. Song, J. Jeong, J.W. Sohn, D. Kim, H.S. Lee, Y. Choe, S. Hwang, and Y. Kang, "Comparative study on energy yield of tunnel oxide passivated contact (topcon) and passivated emitter and rear contact (perc) solar cells and analysis of optimal installation method for vertical photovoltaics," Process Integration and Optimization for Sustainability, 8 (4) 993–1001 (2024). doi:10.1007/S41660-024-00408-4/FIGURES/8.
39) O. Ayadi, B. Rinchi, S. Al-Dahidi, M.E.B. Abdalla, and M. Al-Mahmodi, "Techno-economic assessment of bifacial photovoltaic systems under desert climatic conditions," Sustainability 2024, Vol. 16, Page 6982, 16 (16) 6982 (2024). doi:10.3390/SU16166982.
40) T. Ruan, B. Laumert, and W. Wang, "Techno-economic analysis of urban bifacial pv in high-latitude area," Renew. Energy, 258 124916 (2026). doi:10.1016/J.RENENE.2025.124916.
41) N.H. Baranyai, N. Esses, A. Vincze, and H. Zsiborács, "The effect of orientation and tilt angle on pv system energy production in hungary: regional comparison and optimization possibilities," Discover Sustainability 2025 6:1, 6 (1) 1192- (2025). doi:10.1007/S43621-025-02082-Z.
42) LLC. National Technology and Engineering Solutions of Sandia, "PV performance modeling collaborative (pvpmc) - albedo," (2026). https://pvpmc.sandia.gov/modeling-guide/1-weather-design-inputs/plane-of-array-poa-irradiance/calculating-poa-irradiance/poa-ground-reflected/albedo/ (accessed March 22, 2026).
43) INC. CAMPBELL SCIENTIFIC, "CR1000 measurement and control datalogger," (2026). https://www.campbellsci.com/cr1000 (accessed March 22, 2026).
44) Inc. AnythingWeather Communications, "DS-2 sonic anemometer," (2026). https://store.anythingweather.com/ds-2-sonic-anemometer (accessed March 22, 2026).
45) Inc. Decagon Devices, "DS-2 Sonic Anemometer Operators Manual," 2024. https://metergroup.com/support/downloads-page/meter-environment-archive/?srsltid=AfmBOorUfzA8lGDQjiyWvQgPLcb10jwJutV5bMI1OjDgevfIphsKYuu- (accessed March 24, 2026).
46) Szinker Áruküldő és Kereskedelmi Kft., "Testo 872s thermal imaging camera, iso-calibrated, measurement range: −30 to +650 °c, resolution: 320 × 240 pixels, frame rate: 9 hz (testo 872s hőkamera, iso kalibrált, mérési tartomány: −30 – +650 °c, felbontás: 320 × 240 pixel, képfrekvencia: 9 hz)," (2026). https://www.conrad.hu/hu/p/testo-872s-hokamera-kalibracio-iso-30-650-c-320-x-240-pixel-9-hz-2743439.html?experience=b2c&qwer=Cj0KCQjwpv7NBhCzARIsADkIfWyg_wGlEXOvuQiI9ffbuX2rns8wiJTntOICJMICWr3WfLwnwURT3BEaAn0HEALw_wcB&utm_source=google&utm_medium=cpc&utm_campaign=HU+-+PMAX+-+Nonbrand+-+Invisibles&utm_id=22829107366&gad_source=1&gad_campaignid=22819352346&gbraid=0AAAAAD0MToXaACOEJZRfXm8dOmCyt6MsZ&gclid=Cj0KCQjwpv7NBhCzARIsADkIfWyg_wGlEXOvuQiI9ffbuX2rns8wiJTntOICJMICWr3WfLwnwURT3BEaAn0HEALw_wcB (accessed March 22, 2026).
47) INC. CAMPBELL SCIENTIFIC, "LP02-l pyranometer," (2026). https://www.campbellsci.com/lp02-l (accessed March 22, 2026).
48) Onset Computer Corporation., "HOBO 4-channel analog data logger," (2026). https://www.onsetcomp.com/products/data-loggers/ux120-006m?srsltid=AfmBOopyFk3hD44aLvHseTFhg63lfdBjD9w2bRc1RoWfaYKtE04UNgp2 (accessed March 22, 2026).
49) Victron Energy B.V.;, "SmartSolar mppt 75/10, 75/15, 100/15 & 100/20," (2026). https://www.victronenergy.com/solar-charge-controllers/smartsolar-mppt-75-10-75-15-100-15-100-20 (accessed March 22, 2026).
50) Akku-Fer Sales Kft., "Banner energy bull deep-cycle battery, 12 v, 60 ah, right positive terminal (banner energy bull munkaakkumulátor, 12 v, 60 ah, jobb pozitív saru)," (2026). https://www.auto-motor-akkumulator.hu/Banner-Energy-Bull-12V-60Ah (accessed March 22, 2026).
51) Ltd. JA Solar Technology Co., "JAM72D00 350-370/bp," (2026). https://www.enfsolar.com/pv/panel-datasheet/crystalline/34707 (accessed March 22, 2026).
52) Y. Zhang, J.Q. Gao, Y. Yu, Q. Shi, and Z. Liu, "Influence of incidence angle effects on the performance of bifacial photovoltaic modules considering rear-side reflection," Solar Energy, 245 404–409 (2022). doi:10.1016/J.SOLENER.2022.08.027.
53) N. Riedel-Lyngskær, M. Ribaconka, M. Pó, A. Thorseth, S. Thorsteinsson, C. Dam-Hansen, and M.L. Jakobsen, "The effect of spectral albedo in bifacial photovoltaic performance," Solar Energy, 231 921–935 (2022). doi:10.1016/J.SOLENER.2021.12.023.

Cite: H. Zsiborács, N. Hegedűsné Baranyai, A. Vincze, "Performance Analysis of Bifacial Photovoltaic Modules and Its Practical Implications". Evergreen, 13 (02) 801-812 (2026). https://doi.org/10.5109/7432656.